Effects of Postextrusion Conditions on the Morphology of Foamed High-Density Polyethylene/Polypropylene Blends

C. Zepeda Sahagún,[1] R. González Núñez,[1] D. Rodrigue[2]

[1]*Department of Chemical Engineering, Universidad de Guadalajara, Boulevard General Marcelino García Barragán 1451, Guadalajara, Jalisco 44430, México*
[2]*Department of Chemical Engineering and Centre de Recherche, en Science et Ingénierie des Macromolécules, Université Laval, Quebec City, Quebec GIK 7P4, Canada*

Received 3 November 2005; accepted 8 February 2006
DOI 10.1002/app.24539
Published online 9 July 2007 in Wiley InterScience (www.interscience.wiley.com).

ABSTRACT: The effects of postextrusion conditions (i.e., the draw ratio) were studied to control the cellular structure of extruded foams based on polymer blends. High-density polyethylene and polypropylene were foamed with azodicarbonamide as a chemical blowing agent, zinc oxide as an accelerator, and Kraton D1102 as a compatibilizer. The deformation of the cellular structure and dispersed phase particles was measured with micrographs in both longitudinal and transversal directions to obtain a full three-dimensional picture of the foam morphology. A simple model of the cellular structure is presented to predict cell deformation. © 2007 Wiley Periodicals, Inc. J Appl Polym Sci 106: 1215–1227, 2007

Key words: blends; foam extrusion; morphology

INTRODUCTION

Foaming is a process mainly related to the introduction of small gas cells within a matrix. Foamed plastics are economical alternatives because they can be optimized for stiffness, strength, or energy absorption for a given weight.[1] The mechanical properties of the resulting foams are directly related to the morphology,[2] which is strongly dependent on the processing conditions.[3,4] This is even more critical for polymer blends for which the interfacial tension can be modified by compatibilizers, which change the dispersed phase dimensions and rheological response of the materials. Nevertheless, the individual properties of each polymer composing the blend are of the utmost importance because they control the blend morphology and properties of the resulting foam.[5,6]

The most commonly used materials for thermoplastic foam production are polypropylene (PP) and polyethylene (PE). Because of their high production volume, PE/PP blends are of interest, especially in polymer recycling. For immiscible polymer blends, it has been reported that particles of the dispersed phase can act as foam nucleating agents, enhancing heterogeneous nucleation.[7–13] In most cases, foams based on polymer blends have smaller cell sizes and narrower cell size distributions.

When a polymer blend is foamed, an interaction between the foaming (the introduction of a blowing agent) and blending (the introduction of a second phase) can be observed. For example, Lee et al.[5] found that cell sizes could be changed through the modification of the extrusion pressure, but this had no effect on the size of the dispersed PS domains in high-density polyethylene (HDPE). Furthermore, Lee and Tzoganakis[14] reported that PS domains inside HDPE were smaller and were highly deformed in the flow direction through the dissolution of CO_2, and this resulted in an increased interfacial area between PS and HDPE. This effect was attributed to a lower viscosity ratio (PS viscosity/PE viscosity at 10 s^{-1}), from 2.7 to 1.1, through the dissolution of 5 wt % CO_2 (plasticizing effect of the blowing agent). Modifying the viscosity ratio is known to change the morphology of polymer blends.[15]

On the other hand, Han et al.[16] studied PS foaming with CO_2 and different die temperatures on a twin-screw extruder. The location of the nucleation onset was determined on the basis of the pressure profile and equilibrium solubility. Experimentally, the effects of the cell size, cell density, and cell morphology were investigated at different screw speeds (10–30 rpm). The effect of the foaming temperature on the cell morphology was found to be less significant than a pressure drop, and microcellular PS foams were produced with cells sizes smaller than 10 μm for a die temperature of 160°C, a die pressure drop greater than 16 MPa, and a pressure drop rate higher than 10^9 Pa/s.

Although processing parameters such as the temperature, pressure, and flow rates are important for

Correspondence to: D. Rodrigue (denis.rodrigue@gch.ulaval.ca).

© 2007 Wiley Periodicals, Inc.
WILEY InterScience® DISCOVER SOMETHING GREAT

controlling the foam morphology, the final structure can also be modified and controlled by postprocessing conditions. Some recent studies have been published for polymer blends.

Padilla Lopéz et al.[17] studied numerically and experimentally the deformation of the dispersed phase in PS/HDPE blends produced by ribbon extrusion. Assuming that the deformation was mainly uniaxial, they successfully predicted the ribbon and dispersed particle dimensions at equilibrium. The analysis showed that parameters such as the draw ratio (DR), defined as the takeoff speed divided by the extrusion speed, and ribbon–water contact length (X), defined as the distance between the die exit and water line, significantly influenced the ribbon dimensions and stretching force (stress). The results also showed that the deformation of the dispersed phase and coalescence probability increased for higher DR and lower X values.

Ramirez Arreola et al.[18] studied experimentally and numerically the effect of postextrusion conditions on the final dimensions and morphology of 3, 6, and 9% PS in HDPE produced by ribbon extrusion. In their study, they focused on the DR (1.9–9.4) and water contact distance (3.5–20 cm). They found that the final dimensions of the ribbon (width and thickness) decreased with increasing DR and water contact distance. To predict the ribbon dimensions, nonisothermal numerical simulations were performed with three different rheological models. Although the dimensions of the ribbon were not significantly affected by the rheological model, the stretching force was. Newtonian simulations overpredicted the experimental data, whereas a generalized Newtonian model (Carreau) underestimated them. Good predictions over the whole range of conditions tested were possible only when both elastic and viscous effects were taken into account via the simple Kelvin–Voigt model. Predictions of the final blend morphology (dispersed phase deformation) were also in agreement with experimental data and showed that particle deformation increases with DR but decreases for higher water contact distances. From the definition of the capillary number (Ca), higher stresses (forces) imply larger particle deformation, which is the case with increasing DR and reducing X.

In the case of foaming, Lee et al.[6] studied the extrusion foaming of PS/HDPE blends with CO_2 as the physical blowing agent and found that the dispersed phase sizes decreased with CO_2 addition. The plasticizing effect (viscosity reduction) of CO_2 in both polymers is believed to change the viscosity ratio and the rheology of the blend, leading to a different final size of the dispersed phase.

To the best of our knowledge, there is no literature on the direct quantification of the effects of postextrusion conditions on the full three-dimensional structure of foamed polymer blends. In this article, the influence of DR is presented for PP/HDPE blends and foams produced by extrusion with a chemical foaming agent. The addition of a compatibilizer is also described to determine its effect on blending and foaming. Finally, foam cell deformation is approximated with two simple theories.

EXPERIMENTAL

The materials used in this work were Padmex 65050 HDPE from Pemex, Pro-Fax 6331 PP from Indelpro Petrochemical Alpek Group (Mexico), and a compatibilizer, Kraton D 1102, from Kraton Polymers U.S. LLC (Houston, TX). Azodicarbonamide (ACA) was used as a blowing agent, and zinc oxide (ZnO) was used as an accelerator. Both chemicals were obtained from Electroquímica Mexicana S.A. de C.V.

Foam processing was performed by extrusion via a Haake Rheomix 254 single-screw extruder (diameter = 19 mm and length/diameter = 25). Foams of HDPE and PP blends, with or without 10 wt % Kraton based on the dispersed phase, were also prepared. In all cases, 0.5 wt % ACA and 0.1 wt % ZnO were added for foaming. Runs with 10 wt % Kraton in neat HDPE and PP were also performed to determine any effect of Kraton on foaming. For all cases, the screw rotational speed and total flow rate were kept constant at 23 rpm and 0.83 kg/h, respectively.

The extrusion temperature profile was set to 165, 170, 173, and 175°C from the hopper to the die. In all cases, the water contact line (X = 8 cm and the extrusion velocity (1.02 cm/s) were constant, but the DR was controlled at five levels: 1, 2, 3, 4, and 5. It was not possible to run at DR > 5 because the foams broke and no stable processing conditions were possible. Further details on processing can be obtained from previous studies.[13,19]

The morphology of the resulting foams was exposed in the longitudinal and transversal directions by cryogenic fractures (liquid N_2). Optical microscopy was performed with an Olympus MIC-D to determine the foam cellular structure. Scanning electron microscopy was also performed with a JEOL model JSM 5400 LV to obtain quantitative measurements of the dispersed phase. The pictures were analyzed with Image-Pro Plus version 4.5 (Media Cybernetic). Further details on the experimental method and characterization were reported in a previous article.[13]

The complete viscosity curves of the polymer were obtained by the combination of data at low shear rates with a parallel-plate rheometer (25-mm diameter and 1.5-mm gap) and at high shear rates with a capillary rheometer (length/diameter = 0 or 16). Data were obtained at different temperatures to get

a full characterization of the melts. Capillary measurements were performed on a Rosand Rh-2000 at 175 and 190°C for deformation rates between 12 and 13,000 s^{-1}, whereas frequency sweeps (0.1 and 300 rad/s) at 175, 190, 210, and 230°C were performed under an inert atmosphere (nitrogen) on a Rheometrics ARES rheometer. The test conditions were carefully selected to obtain data in the linear viscoelastic zone of the polymers. The time–temperature superposition was finally used to obtain the HDPE and PP viscosity master curves at a reference temperature of 175°C (die temperature).

Deformation theory

Several models have been developed to predict the deformation of a single particle in a defined flow field (shear or extensional). The models are generally based on Ca, which represents a ratio of viscous and interfacial forces as follows:

$$\mathrm{Ca} = \frac{a\eta\dot{\gamma}}{\sigma} \tag{1}$$

where the interfacial tension (σ), undeformed particle radius (a), and matrix viscosity (η) are related to the flow dynamics via the rate of deformation ($\dot{\gamma}$). Review articles were published by Rallison[20] and Stone[21] on the modeling of particle deformation in shear or elongation.

Unfortunately, correlations are mainly available for small (Ca < 1) or large (Ca > 1) deformations. As presented later in this article, our Ca values are of the order of unity and fall between the limits of application of these theories. To predict the deformation of the foam cellular structure, two simple approaches are presented here: affine deformation and an empirical power law. In our case, cell deformation is related to the L/B ratio, where L is the dimension of the cell in the flow (stretching) direction and B is the average cell dimension in the perpendicular plane (Fig. 1).

Affine deformation

From the definition of $\dot{\gamma}$, the deformation of the polymer melt at the die exit can be approximated as follows:

$$\varepsilon = \int \dot{\varepsilon} dt = \int \frac{dv}{dx} dt = \int_{v_o}^{v_1} \frac{dv}{v} = \ln\left(\frac{v_1}{v_o}\right) = \ln \mathrm{DR} \tag{2}$$

where v is the velocity, ε is the deformation, and $\dot{\varepsilon}$ is the deformation vote.

DR is related to the extrusion velocity (v_o) and the stretching roller speed (v_1) as follows:

$$\mathrm{DR} = \frac{v_1}{v_o} \tag{3}$$

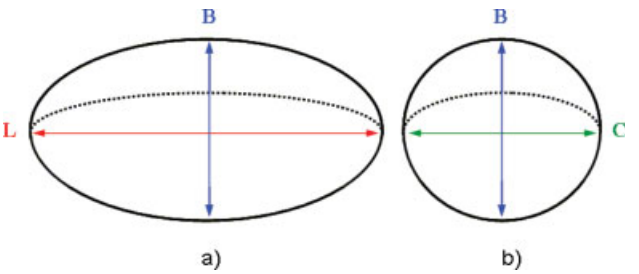

Figure 1 Definition of the cell dimensions: (a) longitudinal (stretching) and (b) transversal (cross-sectional) directions. [Color figure can be viewed in the online issue, which is available at www.interscience.wiley.com.]

If affine deformation is assumed, each gas cell deforms with the polymer melt:

$$\varepsilon = \frac{L - L_o}{L_o} = \frac{L - D}{D} = \frac{L}{D} - 1 \tag{4}$$

where L_o is the initial length, and D is the diameter of the undeformed cell (DR = 1). With the volume conservation criterion, a relation between L/D and L/B can be obtained as follows:

$$\frac{L}{D} = \left(\frac{L}{B}\right)^{2/3} \tag{5}$$

Combining eqs. (2)–(5) gives the following:

$$\frac{L}{B} = (\ln \mathrm{DR} + 1)^{3/2} \tag{6}$$

Empirical power law

Although simple, eq. (6) does not include any physical parameter such as the viscosity or surface tension. As done in the past by Canedo et al.[22] and Hinch and Acrivos[23] for shear and by Hinch and Acrivos[24] for elongational flows, an empirical power-law relation can be obtained between the deformation and Ca as follows:

$$\frac{L}{B} = k\,\mathrm{Ca}^m \tag{7}$$

where k and m are parameters related to the type of flow and range of Ca. From eq. (7), it is clear that the only parameter needed is Ca as defined by eq. (1). Here, some information is needed to calculate the value of Ca. In the case of ribbon extrusion of polymer blends, it has been shown that for short water contact distances, as in our case, the temperature drop between the die exit (X = 0 cm) and water bath (X = 8 cm) is negligible.[18] As a first approximation, all the physical properties of the polymer melt (viscosity and surface tension) are evaluated at the die temperature (175°C), that is, under the assumption of an isothermal process.

TABLE I
Densities (g/cm^3) of the Foamed and Unfoamed Materials

	DR										
	0	1		2		3		4		5	
PP (%)	Unfoamed without Kraton	Foamed without Kraton	Foamed with Kraton	Foamed without Kraton	Foamed with Kraton	Foamed without Kraton	Foamed with Kraton	Foamed without Kraton	Foamed with Kraton	Foamed without Kraton	Foamed with Kraton
0	0.95	0.42	0.49	0.42	0.45	0.37	0.44	0.36	0.43	0.39	0.43
10	0.95	0.41	0.49	0.42	0.45	0.37	0.46	0.38	0.44	0.39	0.43
30	0.94	0.41	0.48	0.42	0.45	0.38	0.45	0.39	0.43	0.38	0.43
50	0.93	0.43	0.49	0.43	0.46	0.38	0.46	0.39	0.44	0.39	0.43
70	0.92	0.41	0.49	0.42	0.45	0.38	0.45	0.37	0.43	0.38	0.43
90	0.91	0.42	0.49	0.42	0.45	0.39	0.45	0.38	0.44	0.38	0.43
100	0.90	0.41	0.48	0.41	0.45	0.39	0.45	0.39	0.43	0.37	0.42

A uniform uniaxial flow approximation is used to evaluate the value of $\dot{\gamma}$ applied to the foaming blend. Our previous study on polymer blends[18] showed that the melt, entering the water bath, rapidly reaches its solidification temperature because of high heat-transfer rates. This freezes the morphology of the material, and no more deformation of the cellular structure is assumed. In that case, an approximation of the deformation rate is

$$\dot{\gamma} = \dot{\varepsilon} = \frac{dv}{dx} \approx \frac{\Delta v}{\Delta x} = \frac{v_1 - v_o}{X} = \left(\frac{v_1 - v_o}{v_o}\right) \frac{v_o}{X} = (DR - 1) \frac{v_o}{X} \quad (8)$$

The undeformed cell radius (a) can be obtained from the average cell volume (V) as follows:

$$a = \left(\frac{3}{4} \frac{V}{\pi}\right)^{1/3} \quad (9)$$

Finally, surface tension (σ) values for both PP and HDPE have been taken from the literature: 26.5 and 22.1 mN/m for HDPE and PP, respectively.[25]

RESULTS AND DISCUSSION

Table I presents the density of each prepared material. First, the foam density is not influenced by the amount of the dispersed phase present in the blend, whereas the unfoamed blend is. This observation is believed to be related to the fact that the final foam density is mainly controlled by the amount of the blowing agent, which was kept constant here. Because the two polymers have similar viscosities (see Fig. 2), the resistance to cell growth is almost the same, and thus the constant foam density is within experimental uncertainty. Second, the density slightly decreases with DR increasing from 1 to 3 as if stretching the matrix helps cell growth up to a point at which almost no difference can be observed by a further increase (4 or 5). Finally, the density is slightly higher when Kraton is added.

Rheological characterization

A rheological master curve of the neat polymers was constructed for a reference temperature of 175°C (die temperature). Figure 2 presents curves in which each set of data has been shifted to the reference temperature with the following Arrhenius relation:

$$a_T = \frac{(\eta_o)_T}{(\eta_o)_{T_o}} = \exp\left[\frac{E_a}{R}\left(\frac{1}{T} - \frac{1}{T_o}\right)\right] \quad (10)$$

The rheological data were then fitted to the generalized Carreau viscosity model as follows:

$$\eta = \frac{\eta_o}{[1 + (\lambda\dot{\gamma})^a]^{(1-n)/a}} \quad (11)$$

where η is power-law index, η_o is zero shear viscosity, and λ is time constant.

Table II reports the numerical values of the parameters in eqs. (10) and (11).

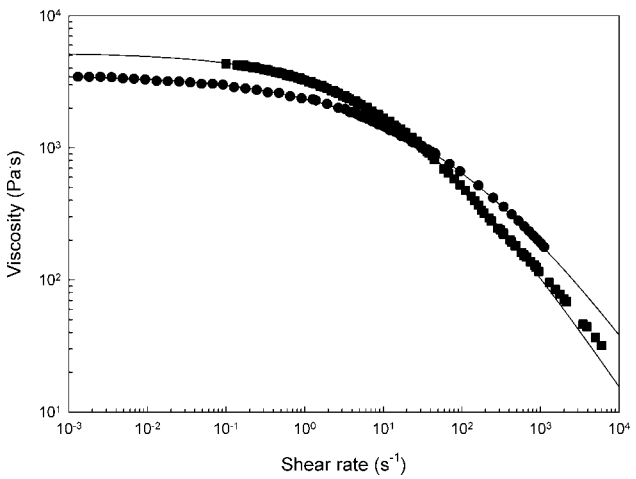

Figure 2 Viscosity master curves of the polymers at a reference temperature of 175°C: (■) PP and (●) HDPE.

TABLE II
Rheological Parameters of HDPE and PP

Parameter	η_o	λ	a	n	E_a/R
Unit	Pa s	s	—	—	K
HDPE	3568	0.0122	0.370	0.133	3242
PP	5238	0.0572	0.454	0.101	4795

Morphological characterization

In this section, we present the dimensions of the cells and dispersed phase particles in both longitudinal and transversal directions. First, Figure 3 presents a typical foam morphology for PP under different DRs (1, 2, and 5). Cell deformation increases substantially in the stretching direction with increasing DR. Tables III and IV report on cell dimensions from longitudinal and transverse directions (L, B, and C), without and with Kraton, respectively. Tables III and IV also report on the average volume of the cells for each condition under study. In general, the longest dimension (L) increases with increasing values of DR, and within the experimental uncertainty, the dimensions in the transverse direction (B and C) are almost equal (see Fig. 1 for the definitions). The effect of the blend composition is again negligible and can be explained by the viscosity of the two polymers used. In Figure 2, the rheological curves of HDPE and PP are very similar, giving a viscosity ratio near unity for the whole range of shear rates. Because the viscosity influences mainly the cell growth, the cell volumes are almost constant. On the other hand, a comparison of Tables III and IV reveals the effect of Kraton addition. It is known that the addition of a copolymer to polymer blends decreases the dispersed phase particle sizes and stabilizes the blend morphology. For a constant concentration of the dispersed phase, a higher number of smaller particles are produced by the addition of Kraton.[26] For foaming, this also increases the total surface area available for cell nucleation. Nucleating a larger number of cells with a constant blowing agent content will consume more rapidly the gas molecules, and full expansion will be reached more quickly.[13] It is clear from Tables III and IV that Kraton addition leads to smaller cells (lower volume), which will influence deformation: smaller cells are more difficult to deform. Furthermore, cell sizes are more uniform and do not change much with the polymer content. Figure 4 presents the effects of the blend composition and Kraton addition on the foam morphology. Kraton addition has an effect even for neat polymers because the copolymer is dispersed as small particles, and this leads to increased heterogeneous nucleation (the copolymer acts as a second phase). To support our discussion on the effect of Kraton on the foam morphology, the dimensions of the dispersed phase particles were also analyzed. Those results are presented next.

In a previous study,[13] the effect of Kraton addition was reported for the same system when no external stretching was applied (DR = 1). From Tables V and VI, it is clear that Kraton addition reduced the volume of the dispersed particles. Because of the high standard deviations (very broad distribution), it is difficult to draw clear conclusions on the effects of foaming and stretching on the dimensions of the dispersed phase in three dimensions. Nevertheless, some general trends can be observed. First, for larger particles (without Kraton), the dimensions in the transverse direction are not equal (lamellar-like structure). The same occurs for the 50/50 composition with Kraton: the volumes with or without Kraton are similar, and this may be related to the phase-inversion effect (at this concentration, the effect of Kraton is negligible). Furthermore, because of the limited amount of space between the cells in a foamed blend, stretching the blends may lead to an increased probability of contact between the particles, and possible coalescence may occur (low interparticle distance). This could explain the increasing volume of the dispersed phase with DR for the 50/50 composition. On the other hand, for lower dispersed phase concentrations such as 10% PP, a higher interparticle distance may limit severely particle coalescence, and particle breakup may take over.

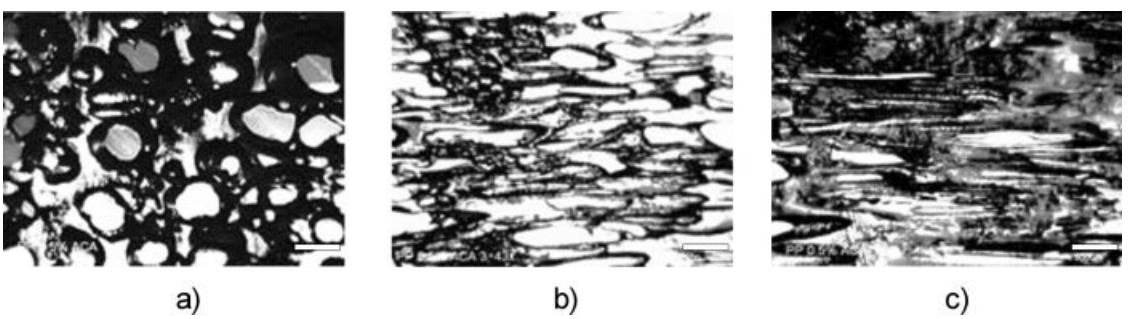

Figure 3 Micrographs in the longitudinal direction of PP foams with different DRs: (a) 1, (b) 2, and (c) 5. The scale bar represents 500 μm.

TABLE III
Foam Cell Dimensions and Volumes for HDPE/PP Blends Without Kraton

	PP (%)																		
	0			10			30			50			70			90			100		
DR	*L* (μm)	*B* (μm)	*C* (μm)	*L* (μm)	*B* (μm)	*C* (μm)	*L* (μm)	*B* (μm)	*C* (μm)	*L* (μm)	*B* (μm)	*C* (μm)	*L* (μm)	*B* (μm)	*C* (μm)	*L* (μm)	*B* (μm)	*C* (μm)	*L* (μm)	*B* (μm)	*C* (μm)
1	172 ± 33	144 ± 20	141 ± 23	192 ± 72	148 ± 57	145 ± 48	164 ± 46	129 ± 25	72 ± 13	158 ± 62	142 ± 34	91 ± 28	159 ± 40	117 ± 23	88 ± 14	244 ± 79	139 ± 58	134 ± 24	257 ± 54	143 ± 42	141 ± 95
2	277 ± 113	120 ± 22	103 ± 42	205 ± 104	147 ± 54	145 ± 44	254 ± 107	115 ± 30	85 ± 21	205 ± 49	98 ± 15	103 ± 18	229 ± 54	116 ± 30	87 ± 24	259 ± 39	133 ± 26	120 ± 26	292 ± 168	72 ± 26	103 ± 41
3	315 ± 105	114 ± 33	84 ± 12	332 ± 115	104 ± 44	104 ± 15	258 ± 67	108 ± 22	108 ± 27	272 ± 104	112 ± 34	80 ± 12	261 ± 65	106 ± 23	97 ± 19	269 ± 53	123 ± 22	108 ± 14	353 ± 129	77 ± 25	85 ± 12
4	322 ± 84	92 ± 26	92 ± 24	452 ± 136	86 ± 43	89 ± 30	308 ± 91	88 ± 25	67 ± 12	362 ± 103	110 ± 22	99 ± 29	330 ± 151	96 ± 21	99 ± 22	320 ± 90	120 ± 16	106 ± 16	489 ± 207	99 ± 26	92 ± 23
5	377 ± 171	104 ± 25	89 ± 14	457 ± 147	114 ± 34	93 ± 31	410 ± 63	64 ± 17	75 ± 18	401 ± 116	111 ± 21	103 ± 41	419 ± 113	114 ± 27	92 ± 21	450 ± 70	127 ± 27	85 ± 20	498 ± 146	72 ± 16	89 ± 14

	Volume (μm^3)						
1	1.8 ± 0.5	2.2 ± 0.4	0.7 ± 0.6	0.7 ± 0.2	0.8 ± 0.5	2.4 ± 0.4	2.7 ± 0.5
2	1.8 ± 0.6	2.0 ± 0.4	1.3 ± 0.2	1.1 ± 0.5	1.2 ± 0.8	2.2 ± 0.2	1.1 ± 0.2
3	1.6 ± 1.1	1.9 ± 0.7	1.6 ± 0.9	1.3 ± 0.2	1.4 ± 0.6	1.9 ± 0.1	1.2 ± 0.3
4	1.4 ± 0.4	1.8 ± 0.4	0.9 ± 0.1	2.0 ± 0.2	1.6 ± 1.0	2.1 ± 0.6	2.3 ± 0.3
5	1.8 ± 0.4	2.5 ± 0.2	1.0 ± 0.6	2.4 ± 0.2	2.3 ± 0.2	2.5 ± 0.2	1.7 ± 0.8

TABLE IV
Foam Cell Dimensions and Volumes for HDPE/PP Blends With Kraton

	PP (%)																		
	0			10			30			50			70			90			100		
DR	*L* (μm)	*B* (μm)	*C* (μm)	*L* (μm)	*B* (μm)	*C* (μm)	*L* (μm)	*B* (μm)	*C* (μm)	*L* (μm)	*B* (μm)	*C* (μm)	*L* (μm)	*B* (μm)	*C* (μm)	*L* (μm)	*B* (μm)	*C* (μm)	*L* (μm)	*B* (μm)	*C* (μm)
1	165 ± 32	132 ± 23	105 ± 20	103 ± 27	76 ± 16	75 ± 8	146 ± 52	106 ± 52	110 ± 30	195 ± 64	141 ± 45	82 ± 16	163 ± 55	97 ± 24	85 ± 11	165 ± 33	99 ± 23	86 ± 13	154 ± 51	133 ± 41	141 ± 90
2	168 ± 42	120 ± 25	100 ± 32	166 ± 35	75 ± 16	83 ± 15	202 ± 66	104 ± 66	113 ± 23	230 ± 63	131 ± 31	76 ± 12	243 ± 95	95 ± 26	82 ± 18	255 ± 38	86 ± 19	86 ± 11	261 ± 97	83 ± 20	109 ± 44
3	226 ± 103	114 ± 35	82 ± 11	186 ± 50	71 ± 12	72 ± 12	277 ± 191	98 ± 29	89 ± 19	300 ± 15	126 ± 16	83 ± 12	316 ± 148	93 ± 55	73 ± 7	264 ± 43	80 ± 14	72 ± 16	309 ± 127	85 ± 25	86 ± 67
4	284 ± 91	93 ± 24	92 ± 23	279 ± 57	70 ± 12	70 ± 9	316 ± 98	89 ± 26	78 ± 17	340 ± 120	117 ± 29	73 ± 20	328 ± 84	87 ± 43	82 ± 16	284 ± 92	75 ± 15	58 ± 11	438 ± 208	90 ± 26	85 ± 38
5	367 ± 172	88 ± 26	80 ± 13	404 ± 89	69 ± 25	63 ± 12	379 ± 193	82 ± 27	46 ± 9	355 ± 78	101 ± 78	65 ± 29	336 ± 228	79 ± 52	60 ± 11	340 ± 113	67 ± 15	75 ± 14	453 ± 184	73 ± 15	83 ± 50

	Volume (μm^3)						
1	1.2 ± 0.7	0.3 ± 0.1	0.9 ± 0.1	1.2 ± 0.3	0.7 ± 0.2	0.7 ± 0.1	1.5 ± 1.4
2	1.1 ± 0.1	0.5 ± 0.1	1.2 ± 0.1	1.2 ± 0.1	1.0 ± 0.4	1.0 ± 0.8	1.1 ± 1.3
3	1.1 ± 0.2	0.5 ± 0.1	1.3 ± 0.1	1.6 ± 0.9	1.1 ± 0.7	0.8 ± 0.6	1.2 ± 0.5
4	1.3 ± 0.1	0.7 ± 0.5	1.2 ± 0.9	1.5 ± 1.1	1.2 ± 1.1	0.7 ± 0.4	1.7 ± 1.1
5	1.3 ± 0.1	0.9 ± 0.7	0.8 ± 0.5	1.2 ± 1.3	0.8 ± 0.6	0.9 ± 0.1	1.4 ± 1.0

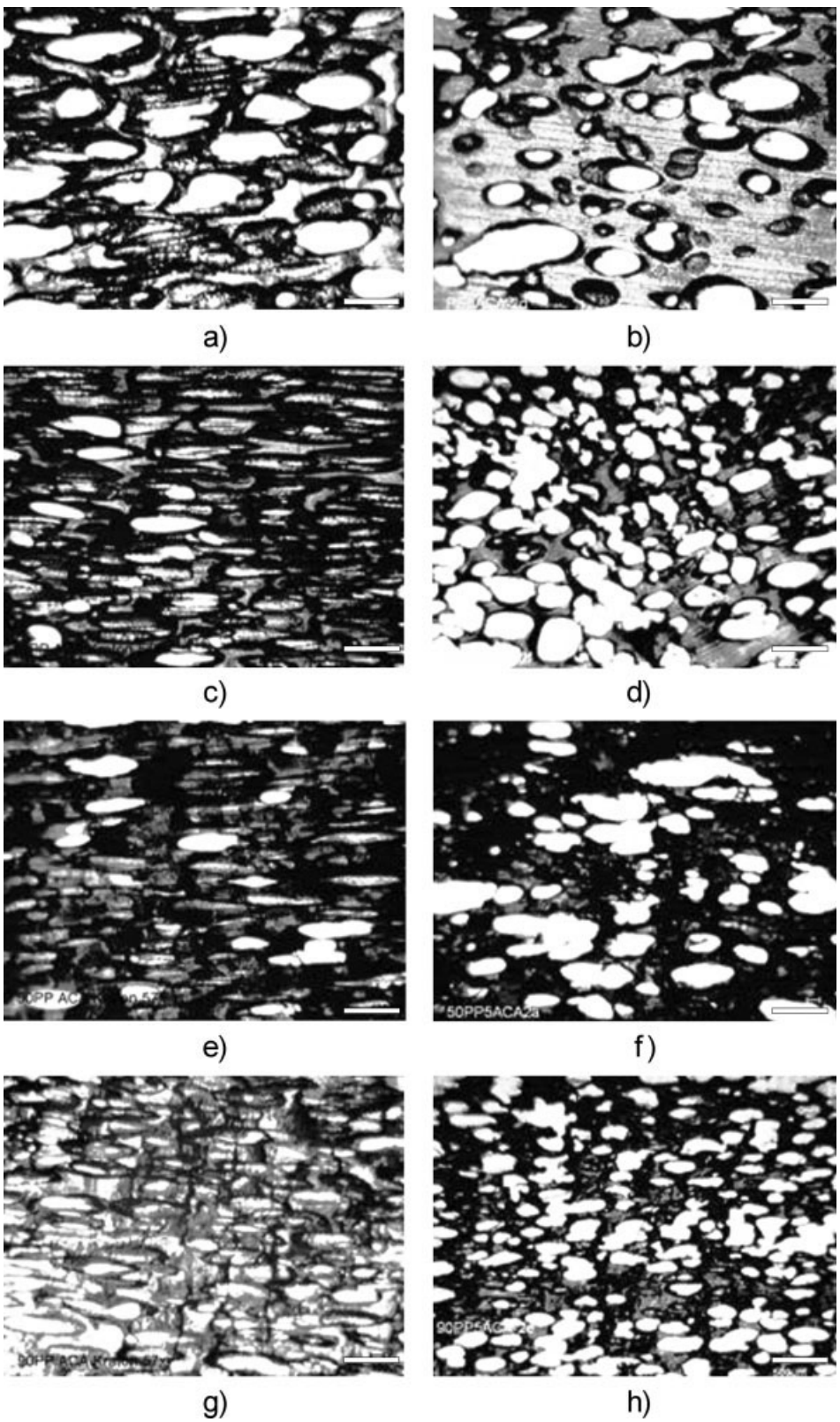

Figure 4 Foam morphology at DR = 2 for different foams: (a) PP, (b) PE, (c) 10% PP without Kraton, (d) 10% PP with Kraton, (e) 50% PP without Kraton, (f) 50% PP with Kraton, (g) 90% PP without Kraton, and (h) 90% PP with Kraton. The scale bar represents 500 μm.

TABLE V
Dispersed Phase Dimensions and Volumes for HDPE/PP Blends Without Kraton

	PP (%)														
	10			30			50			70			90		
DR	*L* (μm)	*B* (μm)	*C* (μm)	*L* (μm)	*B* (μm)	*C* (μm)	*L* (μm)	*B* (μm)	*C* (μm)	*L* (μm)	*B* (μm)	*C* (μm)	*L* (μm)	*B* (μm)	*C* (μm)
1	4.2 ± 1.1	2.3 ± 0.5	0.8 ± 0.1	3.8 ± 1.0	2.1 ± 0.1	0.6 ± 0.1	6.5 ± 2.0	2.3 ± 0.4	1.1 ± 0.7	5.7 ± 0.8	2.2 ± 0.2	0.8 ± 0.2	3.3 ± 0.5	2.3 ± 0.4	0.8 ± 0.4
2	3.3 ± 0.9	2.2 ± 0.5	0.3 ± 0.2	6.6 ± 3.0	2.3 ± 0.4	0.8 ± 0.4	4.6 ± 1.4	1.9 ± 0.2	0.9 ± 0.4	5.7 ± 1.2	2.1 ± 0.4	0.8 ± 0.3	4.4 ± 1.4	2.3 ± 0.4	0.5 ± 0.4
3	3.4 ± 0.7	2.1 ± 0.2	0.6 ± 0.2	6.0 ± 1.1	2.1 ± 0.4	0.7 ± 0.4	6.2 ± 0.6	2.4 ± 0.3	1.0 ± 0.3	6.8 ± 1.9	2.3 ± 0.2	1.0 ± 0.4	4.1 ± 1.7	2.5 ± 0.6	0.5 ± 0.4
4	6.1 ± 2.7	2.0 ± 0.2	0.7 ± 0.5	6.9 ± 1.2	2.6 ± 0.6	0.9 ± 0.6	6.0 ± 1.5	2.0 ± 0.3	0.9 ± 0.3	6.9 ± 2.2	2.5 ± 0.6	0.8 ± 0.4	5.2 ± 1.7	2.2 ± 0.5	0.5 ± 0.5
5	4.0 ± 0.7	1.9 ± 0.1	0.5 ± 0.5	8.5 ± 2.8	2.6 ± 0.4	0.5 ± 0.6	5.2 ± 2.5	2.9 ± 0.7	0.6 ± 0.2	8.5 ± 2.3	2.1 ± 0.3	0.5 ± 0.7	5.3 ± 1.1	2.2 ± 0.4	0.5 ± 0.6
	Volume (μm^3)														
1	4.0 ± 0.3			2.5 ± 1.3			8.6 ± 2.1			5.2 ± 2.4			3.2 ± 1.7		
2	1.1 ± 0.4			6.3 ± 1.6			4.1 ± 2.3			5.0 ± 3.5			2.7 ± 1.8		
3	2.2 ± 1.0			4.6 ± 0.9			7.8 ± 3.4			8.2 ± 1.3			2.7 ± 1.5		
4	4.5 ± 2.0			8.4 ± 1.2			5.7 ± 2.4			7.2 ± 1.5			3.0 ± 1.4		
5	2.0 ± 1.5			5.8 ± 3.2			4.7 ± 1.6			4.7 ± 2.9			3.1 ± 1.1		

TABLE VI
Dispersed Phase Dimensions and Volumes for HDPE/PP Blends With Kraton

	PP (%)														
	10			30			50			70			90		
DR	*L* (μm)	*B* (μm)	*C* (μm)	*L* (μm)	*B* (μm)	*C* (μm)	*L* (μm)	*B* (μm)	*C* (μm)	*L* (μm)	*B* (μm)	*C* (μm)	*L* (μm)	*B* (μm)	*C* (μm)
1	3.0 ± 1.0	1.0 ± 0.3	1.0 ± 0.3	3.4 ± 0.9	1.0 ± 0.3	1.0 ± 0.9	1.7 ± 1.5	1.1 ± 0.4	1.0 ± 0.5	1.6 ± 0.9	2.0 ± 0.2	0.8 ± 0.5	1.5 ± 0.5	1.0 ± 0.2	0.7 ± 0.8
2	2.7 ± 0.3	0.9 ± 0.1	0.9 ± 0.3	3.0 ± 2.9	1.2 ± 0.9	1.2 ± 0.3	2.4 ± 1.9	1.2 ± 0.5	1.3 ± 0.4	2.6 ± 1.4	1.0 ± 0.3	0.7 ± 0.3	1.3 ± 0.2	0.9 ± 0.3	0.7 ± 0.3
3	2.0 ± 0.6	0.8 ± 0.2	0.9 ± 0.2	2.9 ± 1.7	0.9 ± 0.3	0.8 ± 0.3	4.8 ± 1.9	2.1 ± 0.4	1.1 ± 0.4	4.7 ± 1.9	2.0 ± 0.5	0.4 ± 0.2	1.9 ± 0.5	0.9 ± 0.2	0.9 ± 0.2
4	1.8 ± 0.7	1.1 ± 0.2	0.7 ± 0.2	2.1 ± 0.7	1.1 ± 0.2	1.1 ± 0.2	5.5 ± 1.7	2.0 ± 0.3	1.1 ± 0.3	4.4 ± 0.7	1.7 ± 0.2	0.8 ± 0.2	1.4 ± 0.2	0.7 ± 0.1	0.7 ± 0.2
5	1.5 ± 1.0	1.0 ± 0.3	0.8 ± 0.1	1.9 ± 0.6	1.9 ± 0.2	0.8 ± 0.2	8.9 ± 0.4	2.4 ± 0.2	1.1 ± 0.2	3.9 ± 0.9	1.5 ± 0.2	0.7 ± 0.2	1.6 ± 5.6	1.4 ± 0.8	0.8 ± 0.1
	Volume (μm^3)														
1	1.6 ± 1.0			1.8 ± 0.2			1.0 ± 0.9			1.3 ± 0.4			0.6 ± 0.8		
2	1.1 ± 0.6			2.3 ± 0.3			1.9 ± 0.3			1.0 ± 0.3			0.4 ± 0.2		
3	0.8 ± 0.7			1.1 ± 0.1			5.8 ± 0.2			2.0 ± 0.6			0.8 ± 0.1		
4	0.7 ± 0.3			1.3 ± 0.2			6.3 ± 0.3			3.1 ± 0.8			0.4 ± 0.2		
5	0.6 ± 1.0			1.5 ± 0.1			7.2 ± 0.4			2.1 ± 0.7			0.9 ± 0.6		

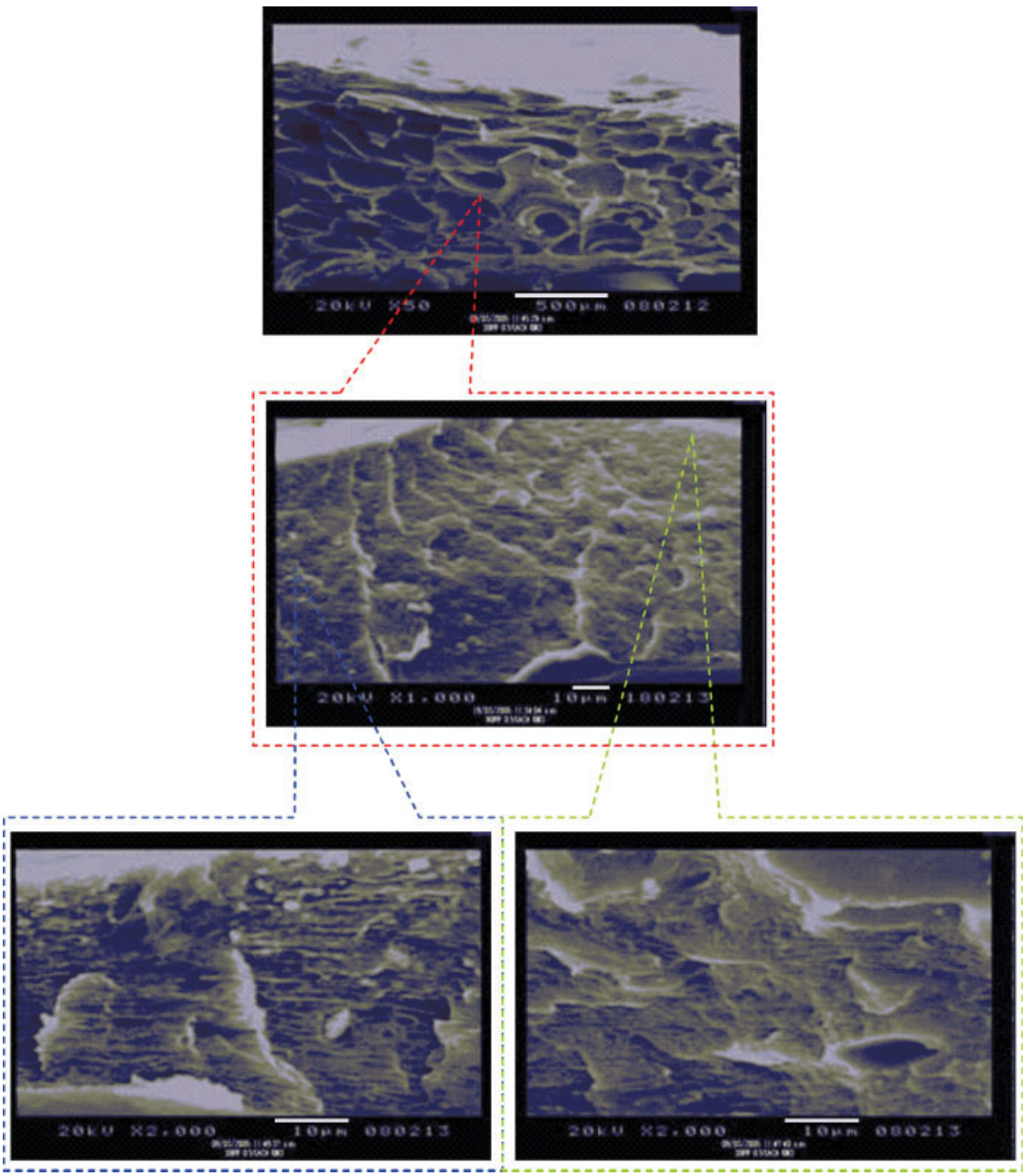

Figure 5 Micrographs of 10% PP foams without Kraton in the longitudinal direction for DR = 3. [Color figure can be viewed in the online issue, which is available at www.interscience.wiley.com.]

This could explain the decreasing particle volume with increasing DR at this composition. The deformation ratio of the dispersed phase (L/B), although not the objective of this article, could be calculated and will be the object of a future report.

Finally, Figures 5–7 present typical micrographs of the foams in both longitudinal and transversal directions, with and without Kraton. Different magnifications enable us to see more clearly the deformation of both phases: cells (gas) and droplets (polymer).

Figure 5 presents some longitudinal micrographs of a foam produced with 10% PP without Kraton for DR = 3. At a magnification of 50× (top), the cellular structure can be determined with clear elongation in the stretching direction (from right to left). At 1000× (middle), the micrograph was taken in the polymer matrix between two cells and indicates some deformation of the dispersed phase around a cell. At 2000× (bottom), it is clear that elongation of the dispersed phase particles is present, but the magnitude and orientation are functions of the position. The picture on the left (between two cells) presents particles that are perfectly aligned with the cell walls, whereas in the picture on the right, the orien-

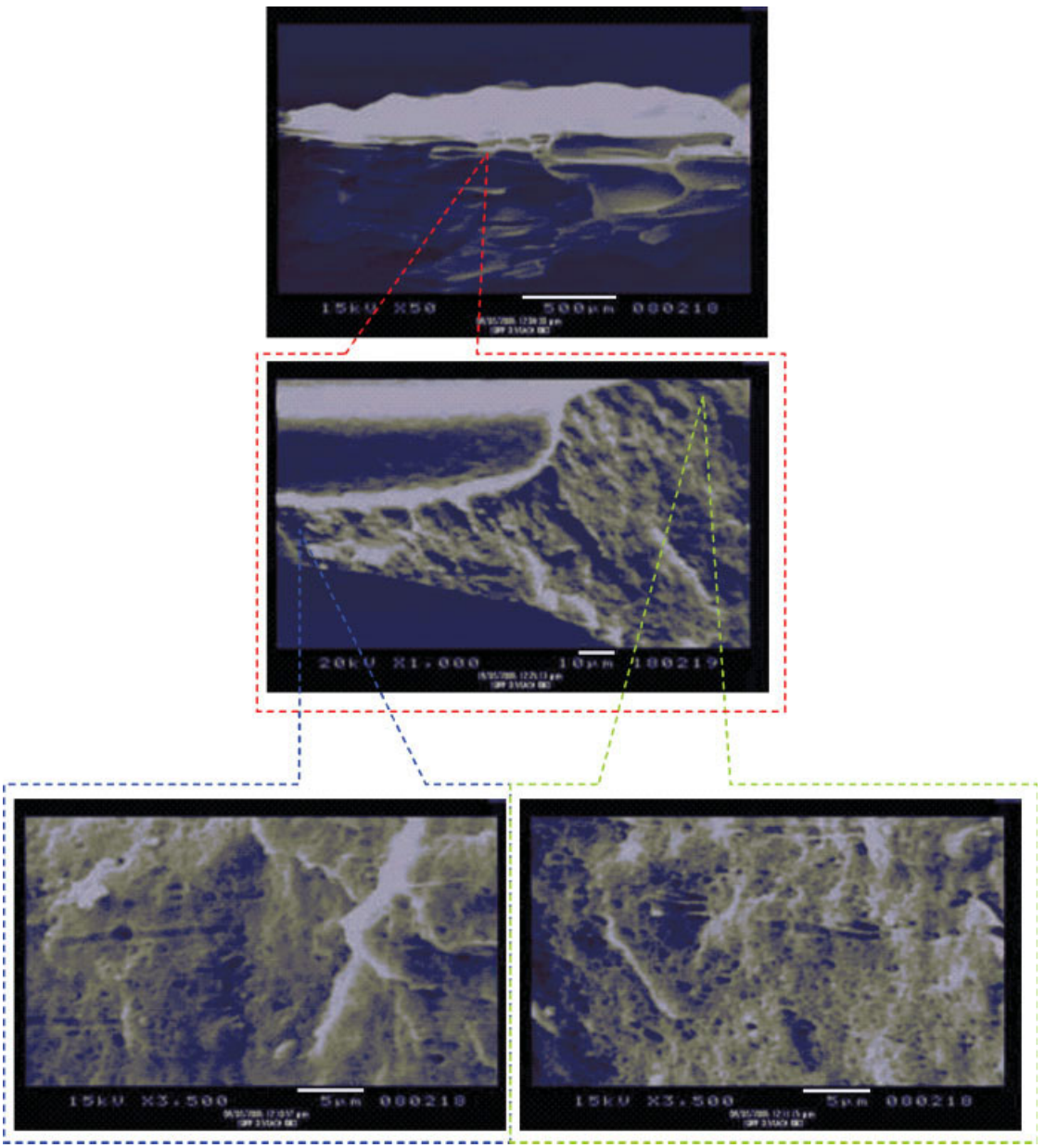

Figure 6 Micrographs of 10% PP foams without Kraton in the transversal direction for DR = 3. [Color figure can be viewed in the online issue, which is available at www.interscience.wiley.com.]

tation is not so clear because of the complex flow between several cells. For comparison, Figure 6 presents micrographs of the same foam in the transverse direction. Because of stretching (DR = 3), the cell and droplet dimensions are smaller, and no clear difference can be seen as a function of the position.

The effect of the position on droplet deformation and orientation is better seen in Figure 7 with Kraton addition. Large deformation can be observed at DR = 3; the bottom left picture presents highly elongated particles almost perfectly aligned in the stretching direction, whereas the picture on the right presents particles at an angle around 45°, indicating a complex flow pattern between polymer stretching and cell growth. It is believed that a combination of elongational and shear flows is responsible for the change in the morphology observed, but this will need further investigation.

From the morphological analysis performed and reported in Tables III–VI, it is now possible to predict, as a first approximation, the deformation of foam cells in relation to postextrusion conditions. Because particles of the dispersed phase (~1 μm) are about 2 orders of magnitude smaller than foam cells (~ 100 μm), their effect on cell deformation is believed to be negligible. In this case, the effect of the dispersed phase will be taken into account only

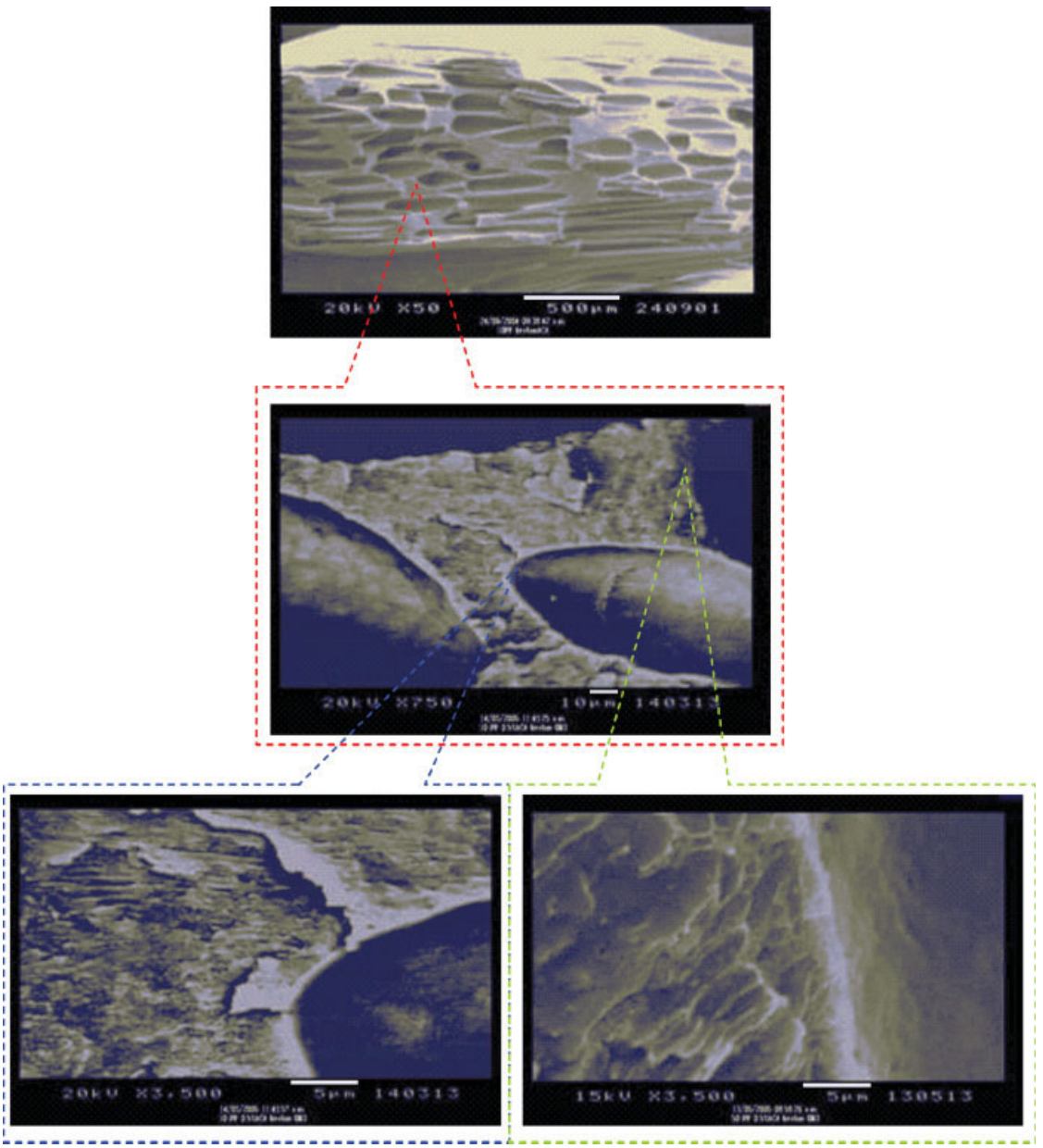

Figure 7 Micrographs of 10% PP foams with Kraton in the longitudinal direction for DR = 3. [Color figure can be viewed in the online issue, which is available at www.interscience.wiley.com.]

via the viscosity of the foaming matrix with the simple mixing rule.

Cell deformation

From the dimensions reported in Tables III and IV, the deformation ratio (L/B) was calculated for each condition studied. In most cases, dimensions B and C in the transverse direction are not significantly different from each other. To simplify the analysis, a surface average dimension was used as follows:

$$B^* = \sqrt{(B\ C)} \tag{12}$$

Figure 8 presents the deformation parameter (L/B^*) for neat HDPE and PP. In general, higher deformations are obtained for neat PP, probably because of its higher viscosity at lower rates of deformation. With eq. (8), the calculated elongational rates are between 0 and 2.85 s^{-1} for DR values between 1 and 5. Because the deformation is related to Ca, a higher value of η leads to a higher deformation ratio. Experiments with 10% Kraton in HDPE and PP were also performed to determine its effect without the presence of a dispersed phase. As shown in Figure 8, deformation is lower when Kraton is added because smaller cell sizes are produced. From earlier

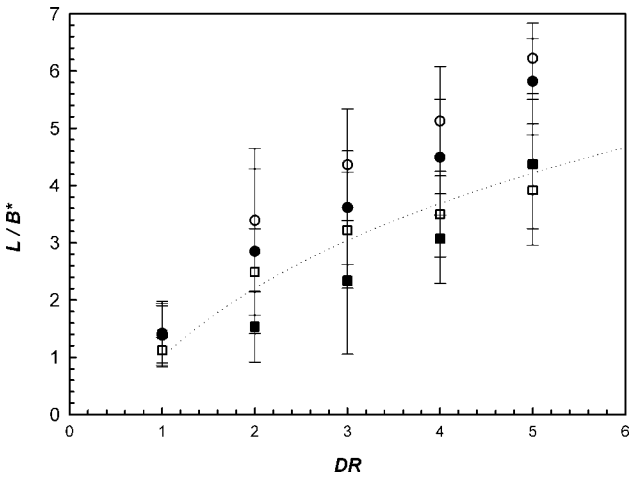

Figure 8 L/B^* as a function of DR: (□) 0% PP and (○) 100% PP. The filled symbols indicate 10% Kraton, and the dashed line was calculated with eq. (6).

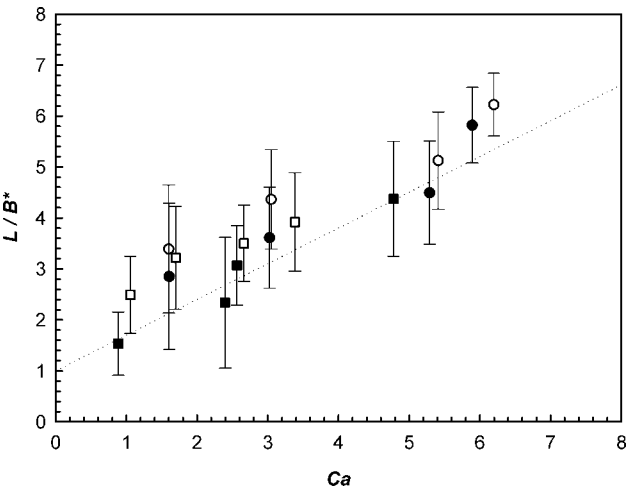

Figure 9 L/B^* versus Ca: (□) 0% PP and (○) 100% PP. The filled symbols indicate 10% Kraton, and the dashed line was calculated with eq. (13).

experiments such as those of Taylor,[27] it is known that smaller particles are more difficult to deform because of higher interfacial stresses (σ/a).

From the simple analysis of affine deformation, eq. (6), as presented in Figure 8, is at best a fair approximation of cell deformation (on average). Nevertheless, the results clearly indicate some dynamic effects because not all the curves superimpose. Physical parameters need to be included, and the Ca analysis is performed next.

In Figure 9, the data of Figure 8 are redrawn as a function of Ca instead of DR. Within the experimental uncertainty, a linear relation is obtained for the range of experimental Ca values ($0 < \text{Ca} < 6$). A modified form of eq. (6) is proposed here to include the limiting case of no deformation ($L/B^* = 1$) when no external stresses are applied (Ca = 0):

$$\frac{L}{B^*} = 1.0 + 0.701\ \text{Ca} \tag{13}$$

Equation (13) being performed for neat polymers (with and without Kraton), a comparison with the blends is performed to determine its validity.

Figure 10 shows that the deformation parameter (L/B^*) of foamed blends with and without Kraton is once again increasing linearly with Ca for the conditions studied. Although standard deviations are large because of broad cell size distributions, the general trend of Figure 9 is valid: increasing DR increases the stresses applied to foam cells, leading to higher deformation.

Figure 10 shows that eq. (13) gives a fair approximation of the deformation ratio for all the conditions tested in this complex situation: extrusion foaming of an immiscible polymer blend, with and without the addition of a compatibilizer, under different DRs. Although the experimental uncertainty is large because of the imprecision of the physical parameters and large distributions of the cell and dispersed phase sizes, the correlation proposed in eq. (13) is a first step toward a better understanding of the parameters controlling the morphology of extruded foams.

CONCLUSIONS

In this work, the effect of DR on the three-dimensional structure of a foamed polymer blend is reported. With HDPE and PP, the foam cell and dispersed phase particle sizes have been measured in

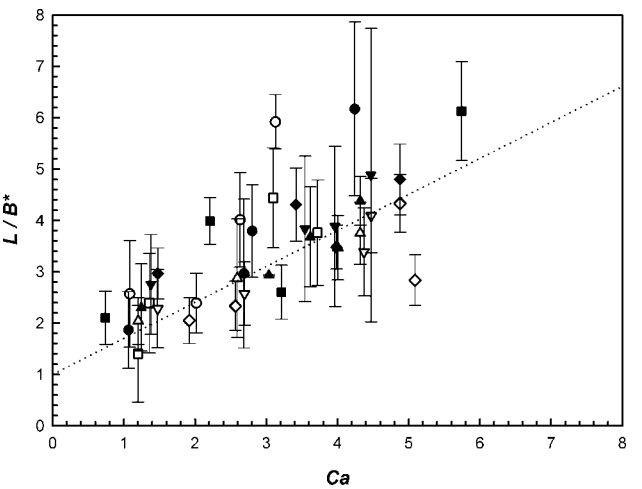

Figure 10 L/B^* versus Ca for foamed blends: (□) 10, (○) 30, (△) 50, (▽) 70, and (◇) 90%. The filled symbols indicate 10% Kraton, and the dashed line was calculated with eq. (13).

both longitudinal and transversal directions. As expected, deformation increases with increasing DR.

With two simple approaches, the deformation of the foam cellular structure has been approximated. The simple affine deformation approach gives at best an average value for the L/B ratio of the cells because the theory does not include any physical property of the components (e.g., surface tension and viscosity). On the other hand, with the Ca approach, a linear relation has been obtained in our range of experimental data. Although not perfect, eq. (13) gives a fair prediction of cell deformation for the range of Ca values obtained for this specific polymer pair. The proposed model is a first step toward a better understanding and control of the cellular structure of foams produced by extrusion in the complex situation in which a polymer blend is used as the matrix.

In the future, further analysis must be performed on the interaction between the blend morphology and foaming. As presented in the micrographs, both the cell and droplet deformations are functions of DR, and further analysis is needed to determine the effects of the rheological properties of each constituent in both shear and elongational flows. Furthermore, because of their relative sizes, droplet deformation and orientation have been shown to be functions of the blend composition and its relative position between the cells. A careful analysis of the flow geometry will enable us to understand the effect of the shear–elongational character of the flow (polymer stretching and cell growth) on particle deformation. Finally, because of cell growth related to the mass transfer and pressure drop, the volume of each gas cell is not constant, and changes in the cell dimensions with time must be included in a future deformation analysis.

One of the authors (D.R.) thanks both Université Laval and Universidad de Guadalajara for financial support for a sabbatical year spent at Universidad de Guadalajara.

References

1. Throne, J. L. Thermoplastics Foams; Sherwood: Hinckley, OH, 1996.
2. Gibson, L. J.; Ashby, M. Cellular Solids: Structure and Properties, 2nd ed.; Cambridge University Press: Cambridge, England, 1997.
3. Lee, S. T. Foam Extrusion; Technomic: Lancaster, PA, 2000.
4. Gendron, R. Thermoplastic Foam Processing. Principles and Development; CRC: Boca Raton, FL, 2005.
5. Lee, M.; Tzoganakis, C.; Park, C. B. Polym Eng Sci 1998, 38, 1112.
6. Lee, C. H.; Lee, K. J.; Jeong, H. G.; Kim, S. W. Adv Polym Technol 2000, 19, 97.
7. Rachtanapun, P.; Selke, S. E. M.; Matuana, L. M. J Appl Polym Sci 2004, 93, 364.
8. Modesti, M.; Adriani, V.; Simioni, F. Polym Eng Sci 2000, 40, 2046.
9. Yang, C. T.; Lee, S. T. Annu Tech Conf Proc Pap 2002, 179.
10. Rachtanapun, P.; Matuana, L. M.; Selke, S. E. M. Annu Tech Conf Proc 2003, 1762.
11. Wan, C.; Xanthos, M.; Dey, S.; Zhang, Q. Annu Tech Conf Proc Pap 2001, 141.
12. Naguib, H. E.; Xu, J. X.; Park, C. B.; Hesse, A.; Panzer, U.; Reichelt, N. Annu Tech Conf Proc Pap 2001, 902.
13. Zepeda Sahagún, C.; González Núñez, R.; Rodrigue D. J Cell Plast, to appear.
14. Lee, M.; Tzoganakis, C. Adv Polym Technol 2000, 19, 300.
15. Vazquez, M. O.; Gloria Bello, O.; González Núñez, R.; Arellano, M.; Moscoso, F. J. Annu Tech Conf Proc Pap 2004, 398.
16. Han, X.; Koelling, K. W.; Tomasko, D. L.; Lee, L. J. Polym Eng Sci 2003, 43, 1206.
17. Padilla Lopéz, H.; Vázquez, M. O.; González Núñez, R.; Rodrigue, D. Polym Eng Sci 2003, 43, 1646.
18. Ramirez Arreola, D.; González-Núñez, R.; Rodrigue, D. Int Polym Proc 2006, 42, 469.
19. Herrera Tejeda, E.; Zepeda Sahagún, C.; González-Núñez, R.; Rodrigue, D. Annu Tech Conf Proc 2004, 3165.
20. Rallison, J. M. Annu Rev Fluid Mech 1984, 16, 45.
21. Stone, H. A. Annu Rev Fluid Mech 1994, 26, 65.
22. Canedo, E. L.; Favelukis, M.; Tadmor, Z.; Talmon, Y. AIChE J 1993, 39, 553.
23. Hinch, E. J.; Acrivos, A. J Fluid Mech 1980, 98, 305.
24. Hinch, E. J.; Acrivos, A. J Fluid Mech 1979, 91, 401.
25. Mark, J. E. Polymer Data Handbook; Oxford University Press: New York, 1999.
26. Technical Data Kraton Polymers for Modification of Thermoplastics; Kraton Polymers: Houston, TX, 2005.
27. Taylor, G. I. Proc R Soc A 1932, 138, 41.